Journal of Natural Gas Science and Engineering xxx (xxxx) xxx

Contents lists available at ScienceDirect

Journal of Natural Gas Science and Engineering

journal homepage: http://www.elsevier.com/locate/jngse

Pillared cloisite 15A as an enhancement filler in polysulfone mixed matrix membranes for CO_2/N_2 and O_2/N_2 gas separation

Phalgun Natarajan [a], B. Sasikumar [a], S. Elakkiya [a], G. Arthanareeswaran [a,*], A.F. Ismail [b], Wirote Youravong [c], Erna Yuliwati [d]

[a] Membrane Research Laboratory, Department of Chemical Engineering, National Institute of Technology, Tiruchirappalli, 620015, India
[b] Advanced Membrane Technology Research Centre (AMTEC), Universiti Teknologi Malaysia, 81310, UTM, Skudai, Johor, Malaysia
[c] Department of Food Technology & Center of Excellence in Membrane Science and Technology, Faculty of Agro-Industry, Prince of Songkla University, Hat Yai, Songkhla, 90110, Thailand
[d] Faculty of Chemical Engineering, Universitas Muhammadiyah Palembang, Palembang, 30263, Indonesia

ARTICLE INFO

Keywords:
Pillared cloisite 15A
Polysulfone
Mixed matrix membranes
Gas permeation
Selectivity

ABSTRACT

The Cloisite 15A (C–15A), an organically modified montmorillonite clay, was further modified with iron (Fe) pillars. Mixed matrix membranes (MMMs) were fabricated by incorporating Fe pillared Cloisite 15A (P–C15A) at different loading percentage of 0.1–1.5 wt% within the polysulfone (PSf) matrix. Fabricated membranes were characterized using thermal studies (TGA and DSC) and scanning electron microscopy (SEM). The morphological studies of fabricated MMMs confirmed that the P–C15A was well embedded through the PSf matrix. To investigate the effect of P–C15A incorporation, MMMs were tested for their gas permeation behavior using pure CO_2, N_2, and O_2 gases. The gas permeation of MMMs was increased with the increase in loading percentage of P–C15A, whereas the gas selectivity was maintained at par to that of neat PSf membrane until it diminished at 1.5 wt% percentage of P–C15A causing mineral agglomeration. PSf/P–C15A (1 wt%) MMMs exhibited 232% and 274% increase in CO_2 and O_2 gas permeability respectively, while showing minimal variation in the selectivity of O_2/N_2 and CO_2/N_2 compared to that of neat PSf membrane. Furthermore, the gas separation performance of neat and P–C15A incorporated MMMs were compared with the Robeson upper bound. The PSf/P–C15A (1 wt%) MMM shown to have CO_2 permeability of 18.01 barrer with the CO_2/N_2 and O_2/N_2 gas pair selectivities of 4.95 and 18.34 respectively, which depicted closeness towards the Robeson upper bound.

Credit author statement

Phalgun Natarajan: Writing – original draft, Methodology B. Sasikumar: Conceptualization, Methodology S. Elakkiya: Conceptualization, Validation G. Arthanareeswaran: Supervision, Writing – review & editing A.F. Ismail: Visualization, Investigation Wirote Youravong: Resources, Writing – review & editing Erna Yuliwat: Resources, Writing – review & editing

1. Introduction

Gas separation is a crucial process in numerous chemical industries that finds its application to produce gasses, gas recovery, and gas treatment (Usman et al., 2019). Compared to conventional separation techniques, membrane separation specifically polymeric membranes have proven to be an exceptional gas separation device owing to their simplicity, minimal energy consumption, modularity, and low cost (Sasikumar et al., 2018) (Dai et al., 2016). Despite these advantages, pure polymeric membranes are restricted by trade–off between gas selectivity and permeability, as explained by the Robeson–upper bound (Robeson, 2008). Researchers are currently developing novel membrane materials to rectify the challenge faced in membrane gas separation and venture closer to the upper bound. One such promising development is the synthesis of MMMs composed of solids embedded into the host polymer matrix. Gas transport through the membranes is generally described by the solution–diffusion mechanism. The mechanism dictates permeant gas dissolve in the membrane and diffuses through the matrix under pressure and concentration gradient (Ismail et al., 2009).

MMMs were fabricated by incorporating various inorganic nanoparticles, including zeolites (Pechar et al., 2006), carbon nanotubes

* Corresponding author.
E-mail address: arthanaree10@yahoo.com (G. Arthanareeswaran).

https://doi.org/10.1016/j.jngse.2020.103720
Received 28 July 2020; Received in revised form 30 October 2020; Accepted 14 November 2020
Available online 19 November 2020

(CNTs) (Kim et al., 2007), silica (Ahn et al., 2008), carbon molecular sieves (CMS) (Vu et al., 2002), and metal oxides (Hosseini et al., 2007), etc. These MMMs exhibit improvement in separation performance at relatively high loadings. Higher loading of inorganic nanoparticles leads to the formation of voids at the particle–polymer interface (Tantekin-Ersolmaz et al., 2000), diminishing mechanical strength of the membrane (Moore and Koros, 2005), and filler agglomeration (Ahn et al., 2008). Clay minerals are a novel filler material that has received significant attention in the fabrication of polymer nanocomposites membranes that enhance their physical and thermomechanical properties though has not been extensively studied as an MMM filler (Guo et al., 2018). A well–used clay mineral is montmorillonite (MMT), a smectite 2:1 clay mineral, with two tetrahedral silica sheets bounding a central octahedral sheet of alumina. The MMT nanoclays incorporated within MMMs have shown significant improvement in gas transport properties at low loading percentage as observed by Herrera-Alonso et al. (2009) and Razaei et al. (Rezaei et al., 2015). Cloisite 15 A (C–15A) is an MMT based clay, organically modified with dimethyl, and dehydrogenated tallow, quaternary ammonium chloride. The organic modification promotes interaction at the polymer-filler interface. Further, the greater interlayer space ensures enhanced dispersion. Compared to other clays, C–15A based MMMs have consistently shown better gas transport properties (Zulhairun and Ismail, 2014) (Hashemifard et al., 2011).

Pillared clays (PILCs) are an exciting modification of smectite clays exhibiting microporosity (Mnasri-Ghnimi and Frini-Srasra, 2014) wherein clay layers are separated and held apart by inorganic polyoxocations, known as pillars (Johnson et al., 1996). PILCs exhibit pore sizes in the micropore range, rendering them suitable for gas separation (Vercauteren et al., 1996). Vercauteren et al. investigated single gas permeation properties of ceramic membrane with top layer alumina pillared montmorillonite clay (Vercauteren et al., 1998). The ceramic membranes were prepared by immersing the support layer in clay suspension and subsequently in alumina pillaring solution. However, the gas permeation test specified high gas flow resistance owing to incomplete pillaring process and the existence of unpillared clay over the ceramic membrane top layer. The drawback of ceramic membranes can be conquered by the usage of pillared clay within the polymeric membranes. To the best of our knowledge, no studies were conducted on P–C15A incorporated polymeric MMMs for gas separation studies.

PILCs are porous nanoparticles mainly used for adsorption and catalysis studies. Generally, montmorillite (bentonite) was commonly used as base material for synthesis of pillared clay. C–15A, an organo-modified montmorillite was not yet used for pillaring process. In this research work, C–15A was used as novel base material for synthesis of iron pillared Cloisite 15A (P–C15A) and used for gas separation studies. The extent of pillaring can be controlled as per micropore volume and surface area requirements (Johnson et al., 1996). Iron (Fe) pillaring with bentonite has been successfully conducted by titrating sodium hydroxide (NaOH) with ferric chloride ($FeCl_3$) shown better results with an OH/Fe ratio of 2 (Valverde et al., 2005). The improvement in micropore volume and surface areas of various Fe and Al pillared clays are displayed in Table 1. PILCs also exhibit excellent thermal stability, which is a crucial requirement for gas separation membranes (Li et al., 2018).

Table 1
Microporous surface area and volume of pillared clay compared to unmodified clay.

Unmodified Clay	S_{micro} (m^2/g)	V_{micro} (cm^3/g)	PILC	S_{micro} (m^2/g)	V_{micro} (cm^3/g)	References
Bentonite	15	0.003	Fe-PILC 2	285	0.126	Valverde et al. (2005)
Montmorillonite	18.5	0.004	Mt. Al–Fe	202	0.034	Mandalia et al. (1998)
Montmorillonite	18.5	0.004	Mt. Al	246	0.104	Mandalia et al. (1998)
Bentonite	19	0.01	Al–PILC	195	0.1	Matteucci et al. (2006)

Glassy polymers have received significant attention for gas separation owing to their mechanical properties and economical advantages (Park and Paul, 1997). PSf has been selected for the polymer matrix, as it is an extensively studied commercially available glassy polymer exhibiting favorable permeability–selectivity characteristics (Ismail et al., 2009), and robust chemical stability (Ismail and Lai, 2003), and high thermal stability. In addition, the high solubility of PSf with a good film forming properties, render it advantageous for membrane applications. In Section 1, the importance and novelty of the work have been discussed. section 2 deals with the experimental setup, and the procedures followed to fabricate the novel P–C15A incorporated PSf/P–C15A MMMs, in addition to the methods employed for MMMs characterization. Furthermore, section 3 describes the results and discussion involving membrane characterization, and effect of P–C15A addition on the PSf MMMs for gas transport studies of CO_2, N_2 and O_2 gases in terms of permeance and selectivity. Results of the fabricated MMMs were further compared with literatures, and the Robeson upper bound. Section 4 concludes the results, and defining the future scope of P–C15A MMMs studies.

2. Experimental

2.1. Materials

MMMs were synthesized, wherein the continuous polymer phase was composed of Polysulfone (PSf, Grade–3500), by Amoco Chemicals, USA, which is a strong thermoplastic, soluble in dipolar solvents, well suited for fabricating high strength membranes. The solvents used for the dope solution preparation were Tetrahydrofuran (THF, 99.5% purity), obtained from QReC, New Zealand. ACROS, Belgium supplied N-Methyl-2-Pyrrolidone (NMP, 99.5% purity). Ethanol (100% purity) was procured from Hayman Limited, UK, which was used as a non-solvent additive and methanol (99% purity) were procured from Sigma-Aldrich, USA. Cloisite 15A was provided by Southern Clay Products, Inc., USA. Polydimethylsiloxane (PDMS, Sylgard 184) for membrane coating was procured from Dow Chemicals, USA.

2.2. Preparation of Fe pillared–Cloisite 15A

P–C15A was prepared by using a pillaring solution, as described by Timofeeva et al. (2009) (Timofeeva et al., 2005). The pillaring solution was synthesized by initially preparing equal quantities of 0.4 M NaOH solution, and 0.2 M $FeCl_3$ solution, to ensure a 2:1 OH/Fe ratio (Valverde et al., 2005). The NaOH solution was added drop by drop at 1 ml/min to the $FeCl_3$ solution. The solution was kept stirring and allowed to age for 24 h at room temperature. C–15A was consequentially added to distilled water at a ratio of 4g of C–15A per 100 ml distilled water, and stirred for 2 h, ensuring uniform dispersion. The C–15A suspension is then added to the pillaring solution and continuously stirred to age 48 h. Then the solution was vacuum filtered until the pillared clay was obtained. The pillared clay denoted as P–C15A after calcination in an oven at 80 °C for 8h. The schematic of the preparation of Fe pillared–Cloisite 15A is presented in Fig. 1.

2.3. Preparation of dope solution

An asymmetric flat sheet MMMs were prepared from the dope solution consisting of PSf (30 wt %), NMP (30 wt %), THF (30 wt %), ethanol (10 wt %) and, P–C15A (0.1–1.5 wt %). THF was used as a volatile solvent to prevent large unselective macro–voids during the instantaneous demixing. Ethanol was used as a non–solvent added drop by drop for post homogenization of dope solution to improve the polymer–polymer interaction, and facilitate rapid polymer solidification

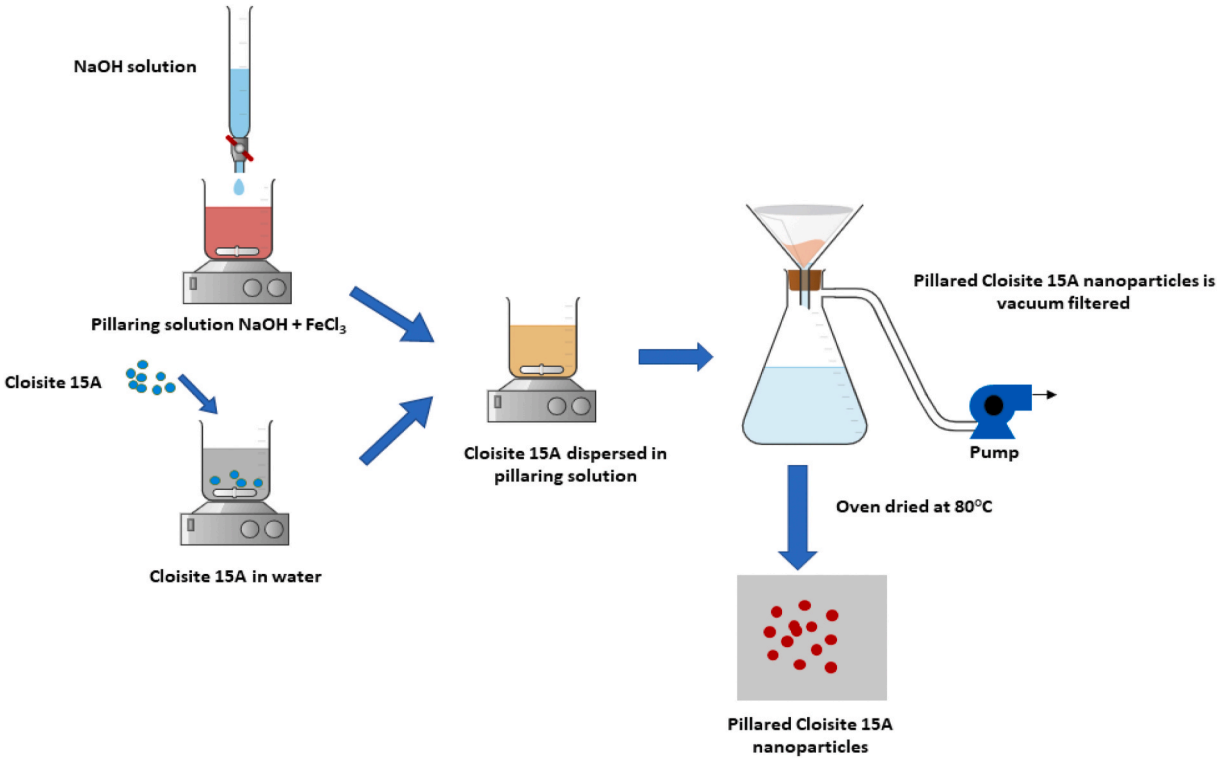

Fig. 1. Schematic representation of pillared cloisite 15A synthesis.

during casting (Aroon et al., 2010). The P–C15A was added to the solvents NMP and THF stirred for 10 min and ultrasonicated for 20 min at 60 °C. Initially, 10 wt % of total PSf polymer was added and stirred for 4 h under constant heating at 60 °C to ensure the wetting of filler particles. Remaining PSf polymer was gradually added and mixed till homogenization was achieved. Ethanol was added dropwise under constant stirring (Aroon et al., 2010) (Zulhairun et al., 2014), and the complete fabrication process was depicted in Fig. 2.

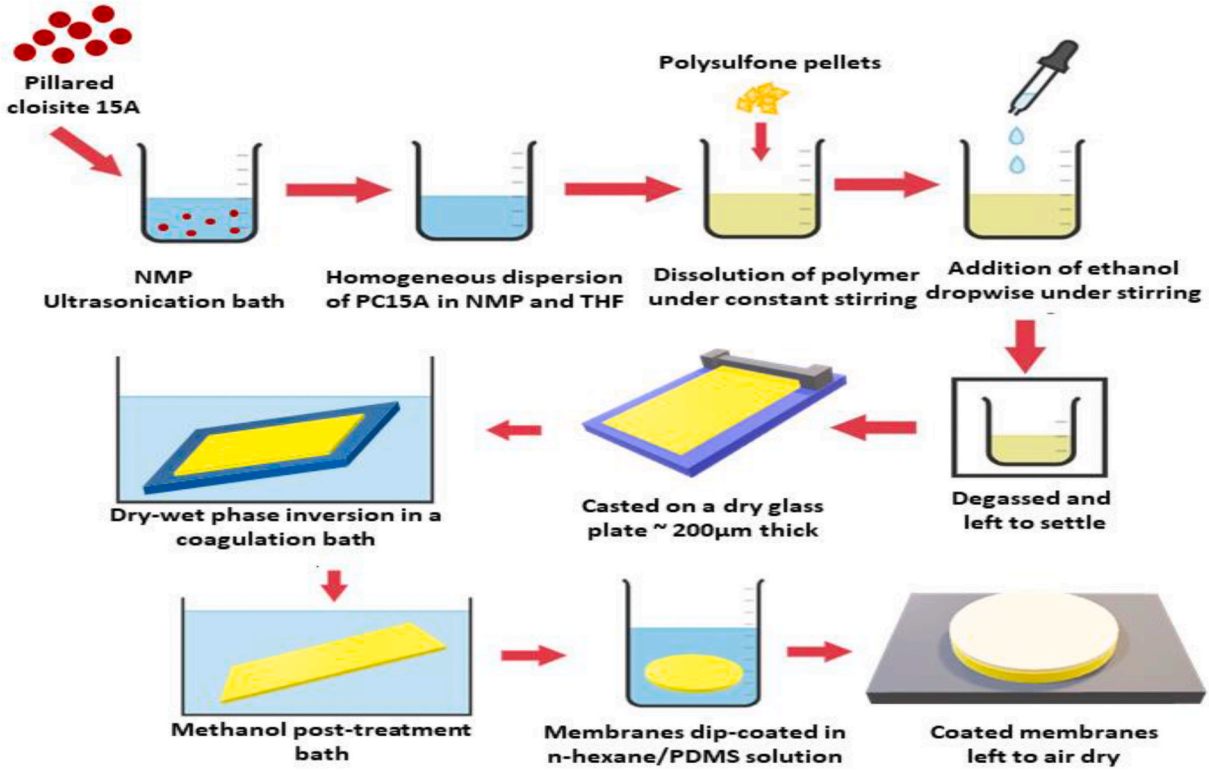

Fig. 2. Schematic representation of membrane casting procedure.

2.4. Fabrication of P–C15/Polysulfone MMMs

The dry–wet phase inversion technique was employed to cast MMMs as per methods followed in (Aroon et al., 2010) (Zulhairun et al., 2014). The prepared solution was poured on a sterilized glass plate and spread evenly by a casting knife of thickness about 200 μm. The casted membrane was left in air for 10 s, and immersed in a distilled water coagulation bath to allow for the dissipation of the solvents from the membrane that facilitated the pore-forming process. The membrane was left immersed in the coagulation bath for 48 h. Post–treatment was conducted on the membranes before further drying.

2.5. Post–treatment of MMMs

Methanol treatment aids in the removal of residual solvent and allows relaxation of polymer chains and improves permeability. The post–treatment of the membranes was commenced immediately after extracting the membranes from the coagulation bath. The membranes were kept immersed for 2.5 h in methanol bath and dried at room temperature for 48 h.

2.6. PDMS coating of MMMs

PDMS is a polymeric organosilicon compound with low selectivity and high permeability due to their higher flexibility of siloxane chain linkages (Pandey and Chauhan, 2001). PDMS is chemically inert, flexible, and exhibits good adhesive properties. This silicone rubber polymer (Dow Corning Sylgard 184) was implemented to coat the membranes. PDMS coating ensures the membranes to be defect–free, uniform top surface, free from pinholes and abrasions. These properties improve membrane selectivity and performance. PDMS coating was executed by dip–coating, similar to the methods described in (Zulhairun et al., 2014). The membranes were plunged in an n–hexane solution with 3% w/w PDMS for 10 min and subsequently removed. The coated membranes were left undisturbed to cure at atmospheric conditions overnight. The neat PSf membrane was fabricated by following the above procedure without incorporating P–C15A in the dope solution. The neat and P–C15A incorporated MMMs were denoted as PSf, PSf/P–C15A (0.1 wt%), PSf/P–C15A (0.5 wt%), PSf/P–C15A (1 wt%), and PSf/P–C15A (1.5 wt%).

2.7. Characterization of P–C15A/polysulfone MMMs

The surface morphology and the elemental composition of C15A and P–C15A were examined using SEM equipped with energy–dispersive X–ray (SEM–EDX, Oxford Instruments INCA PentaFET–X3, UK) (Ghasemipour et al., 2020) (Rezaee et al., 2016). Thermal stability of neat and MMMs was tested using a thermogravimetric analyzer (TGA, DGT, 2000; PerkinElmer, USA). The parameters set for the TGA analysis between temperature ranges of 40–600 °C at a heating rate of 10 °C/min under N_2 atmosphere with an N_2 flow rate of 20 ml/min. A differential scanning calorimeter (DSC, 6000-Perkin-Elmer instrument, USA) was employed to identify the fabricated membranes glass transition temperature (T_g). The membrane samples were made into finely cut pieces and placed into a pre-weighed aluminum crucible. The samples were then heated from a temperature range of 30–400 °C. The glass transition region is recorded, and the transition region's midpoint was taken as T_g. The top and cross–sectional morphology of neat and MMMs were analyzed using SEM (TM 3000, Hitachi). Before testing, the samples were cryogenically fractured under liquid nitrogen. Further, the surfaces of the samples were coated with platinum by sputtering for facilitating electrical conductivity.

2.8. Gas transport properties

Separation efficiency was evaluated by the quantification of permeabilities and selectivities of the neat and MMMs. Gases such as O_2, CO_2, and N_2 with 99.99% purity were utilized to conduct the single gas permeation test. Circular disc is mounted on the top of a stainless–steel permeation unit of the constant pressure system. The experimental setup used is a constant pressure variable volume setup, and the schematic diagram given in Fig. 3. The dependent driving force factors in the adsorption, diffusion, and desorption of the gas molecules for its separation are pressure (ΔP) and temperature (ΔT). The membrane was calculated at constant pressure and temperature of 4 bar and 25 °C, respectively. A soap bubble meter was attached near the exit of gas permeate to measure the gas flux by measuring the volume of permeate gasses per unit time.

Permeance was calculated using equation 1

$$\frac{P_i}{l} = \frac{Q}{A\Delta P} \tag{1}$$

where, Pi/l is defined as the permeance for penetrating gas and is measure in GPU. Q is the flow rate of gas entering, ΔP is pressure drop across the membrane, A is exposed surface area of the membrane, and l is skin thickness of the membrane. The permeability could be evaluated in Barrer. ($1\ Barrer = 1 \times 10^{-10}\ cm^3\ (STP) cm\ /cm^2\ s\ cmHg$).

Selectivity $\alpha_{a/b}$of gases is defined as the ratio of the permeabilities of two gases. It is the metric to determine the potential efficiency of the gas separation of the gasses. Selectivity is calculated using equation (2).

$$\alpha_{a/b} = \frac{(P_a/l)}{(P_b/l)} \tag{2}$$

where, Pa/l refers to the observed permeance of the first gas through the membrane, and Pb/l refers to the experimentally observed permeance of the second gas through the membrane. The selectivity of two gasses is based on the kinematic diameter of the molecules. The gasses exhibiting lower kinematic diameters tend to dissipate through the membrane pores faster than the gas molecules with larger kinematic diameters. N_2 possesses larger kinematic diameter compared to O_2 and CO_2, hence N_2 permeates at a slower rate.

3. Results and discussion

3.1. SEM–EDAX analysis of C15A and P–C15A

Morphology of the C–15A and P–C15A were presented in Fig. 4. The C–15A exhibits as irregular layered silicate structure and was lumped together. Whereas, pillared clay (P–C15A) dispersed as porous material with fluffy appearance. Upon the pillaring process, the close perspective indicates the silicate layers of P–C15A become swollen and appeared in segregated manner. EDAX spectroscopy was conducted to obtain the filler particles elemental composition both prior and post–modification. Fig. 5 depicts the EDAX spectrum and indicates the composition of the denoted elements in the filler particles. The corresponding atomic fractions are displayed in Table 2. In P–C15A, an increase in Fe atomic percentage of about 76% was observed compared to C–15A. In P–C15A, there is an interaction between Fe cations and the C–15A layers (Kurian and Babu, 2013). Further, there is a decrease in the Si/Al ratio of the pillared clay in comparison to C–15 A, indicating an increase in total pore volume and surface area, contributing to the pillaring effect (Gil et al., 2005). The minor decrease in Al and Si elemental composition in P–C15A is due to the replacement of cations from the gallery interlayer as an additional consequence of the iron pillaring procedure.

3.2. Surface morphology of neat and PSf/P–C15A MMMs

SEM images of the top surface and cross–section morphology of the neat and MMMs were illustrated in Fig. 6 and Fig. 7, respectively. Analysis of top surface images of all membranes reveals smooth surface structure. From Fig. 6, MMMs loaded with P–C15A (up to 1 wt%) show homogeneous dispersion of filler on the top surface. Because of the

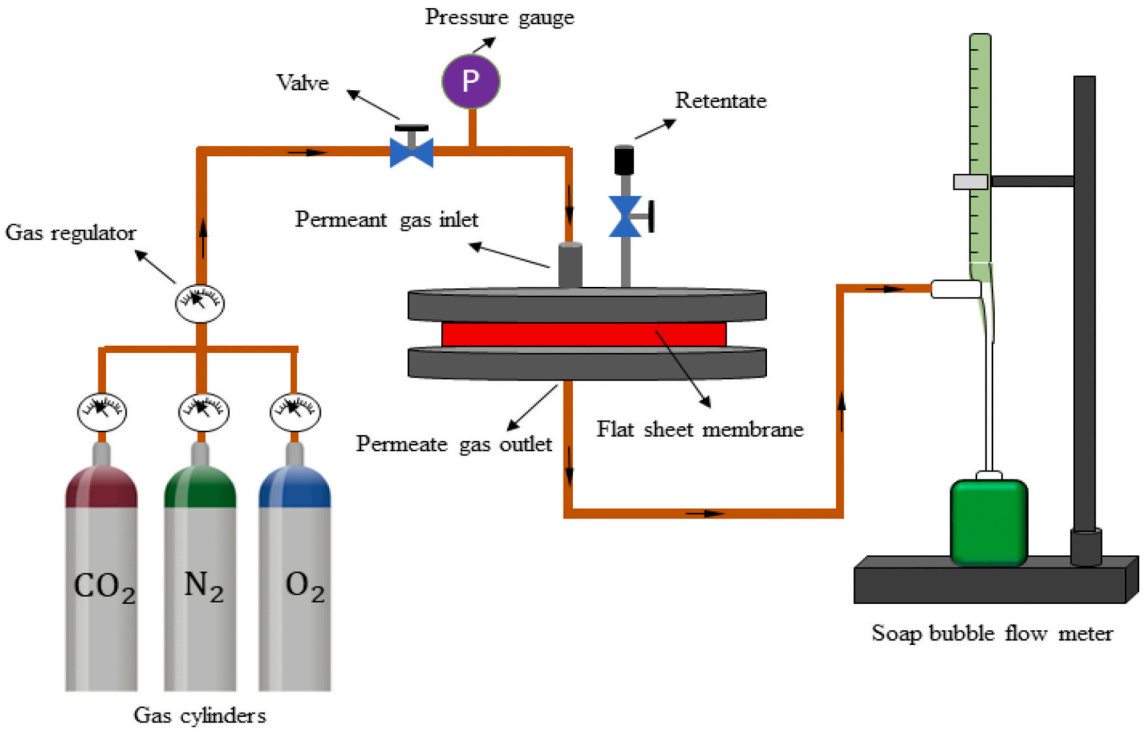

Fig. 3. Gas permeation testing setup.

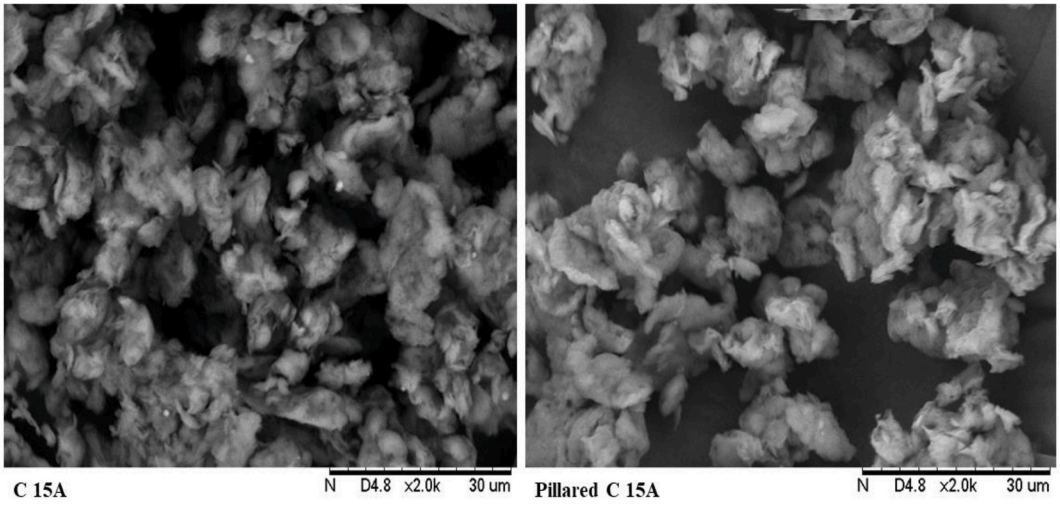

Fig. 4. SEM images of Cloisite 15A and Pillared Cloisite 15A.

compatibility between filler and polymer, surface defects were not seen in MMMs that ensure optimal gas transport properties. At higher P–C15A loading percentage, PSf/P–C15A (1.5 wt%) membranes displayed white traces, indicating that the filler particles obviously protrude in the MMMs surface. As anticipated, all membranes exhibit asymmetrical structure which effectively fabricated by dry–wet phase inversion technique. In Fig. 7, MMMs morphology reveals a well-defined and structural defect free thin dense selective skin layer supported with porous sub sublayer structure containing finger-like macro voids surrounded by trace spongy-like structure (Zulhairun and Ismail, 2014). The thin surface layer is attributed to volatile solvent's addition to a dope solution resulting in quick diffusion during casting. The spongy appearance of the microporous region was attributed to non–solvent ethanol to the solution (Moaddeb and Koros, 1997). Membrane morphological properties slightly vary with the P–C15A nanoparticles at different loading concentration. Due to the low loading of filler particles (<1.5 wt%), it was difficult to detect the individual filler particles, though changes in membranes morphologies were evident. Cross sections of MMMs fabricated with different P–C15A loadings confirm the homogeneity, P–C15A dispersion and the intimate assimilation of filler within the PSf matrix. Absence of significant defects in the top surface and cross–section morphology of PSf/P–C15A membranes up to 1 wt% loading was due to excellent adhesion between the P–C15A and PSf matrix. The filler's superior adhesion was attributed to the modification of C15A with Fe pillar via pillaring treatment (Aroon et al., 2010). Accordingly, the effective pore volume within the polymer membrane matrix leads to substantially increase gas permeability without noteworthy loss in membrane selectivity. Hence, the ideal morphology of PSf/P–C15A (1 wt%) enhances permeance and selectivity. For high loading of P–C15A (1.5 wt%), the formation of finger-like macro voids

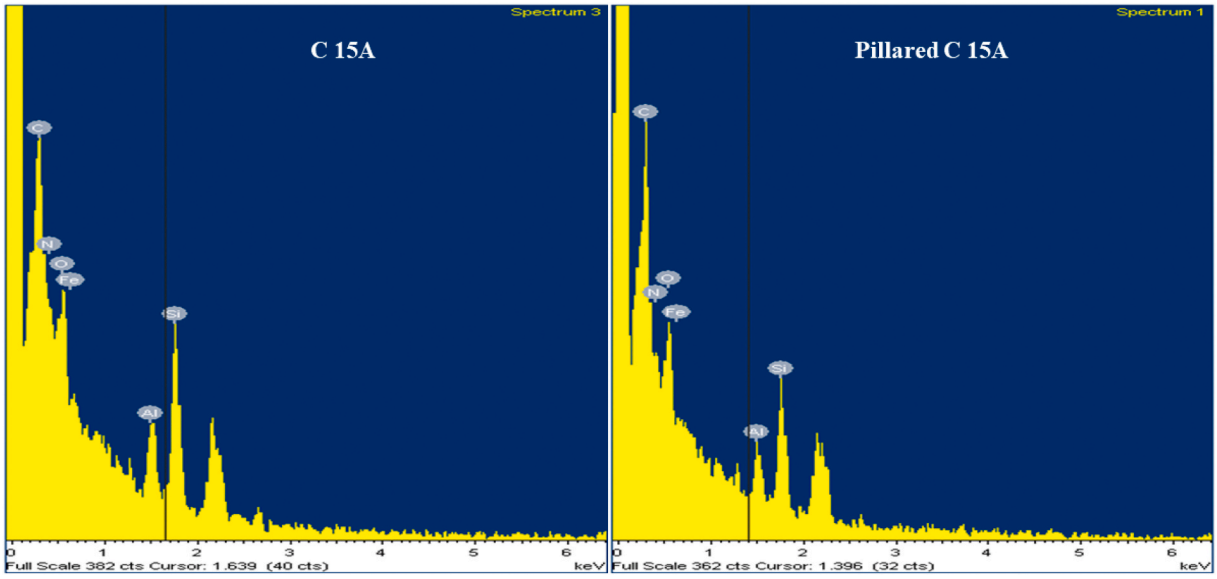

Fig. 5. Edax of cloisite 15A and pillared cloisite 15A.

Table 2
Atomic percentage of Fe, Al, and Si in C–15A and P–C15A.

Sample name	Fe	Al	Si
C–15A	0.26	2.07	4.74
P–C15A	0.46	1.92	4.14

structure was suppressed and becomes bulbous owing to the delayed demixing during phase inversion technique. Consequently, there may be defect in specific membrane structure leads to variation from the membrane ideal morphology. This variation may affect the membrane selectivity for gas pairs. It was observed that with the addition of filler particles, there is a correlating linear increase in the magnitude of macro void formation in the membrane's structure. The development of selective voids in the microporous region is anticipated to increase the gas permeation rate through the membranes.

3.3. Thermal stability of neat and PSf/P–C15A MMMs

TGA results of the neat and PSf/P–C15A MMMs were displayed in Fig. 8. The weight loss occurred below 100 °C is attributed towards desorption of water molecule (Fattahi et al., 2015). The TGA thermographs of all membranes revealed a single significant weight loss. The onset degradation temperature for the neat membrane was 469 °C, and the primary significant diminishment in weight observed between 500 and 540 °C was consistent with the literature for neat PSf membranes (Sasikumar et al., 2019). The weight loss takes place from 500 °C ascribed towards thermal decomposition of PSf polymer backbone. The thermal degradation range was very similar for neat and PSf/P–C15A MMMs owing to low loading (<1.5 wt%). Nonetheless, the analysis of thermal degradation midpoint follows a slightly increasing trend with the loading of P–C15A. This was attributed to the intrinsic high thermal stability of the filler particles. The pillaring of clay has been noted to enhance the thermal stability of clays (Li et al., 2018). These thermostable clay layers dispersed within the polymer matrix increased the degradation temperature (Unnikrishnan et al., 2012). The weight loss occurs in a single phase with a linear fashion, indicating no residual solvent content entrapped in the membrane samples. Only negligible thermal degradation of filler was observed, owing to the low volume fractions incorporated within the MMMs. The residual solvent was successfully removed through the post–treatment of the membranes.

3.4. DSC analysis of neat and PSf/P–C15A MMMs

Thermal properties of neat and MMMs were studied using DSC analysis to evaluate P–C15A loading on the glass transition temperature (T_g) and it is illustrated in Fig. 9. The Tg of the neat PSf membrane was 179.11 °C, which was consistent with the literature (Sasikumar et al., 2019). In case of PSf/P–C15A (0.5 wt%), PSf/P–C15A (1 wt%), and PSf/P–C15A (1.5 wt%) membranes, the T_g was found to be 180.03 °C, 181.54 °C, and 182.76 °C respectively, which shows that MMMs are more stable than the neat PSf membrane. The T_g was increased slightly with the increase in P–C15A loading percentage and a similar trend has been reported earlier (Rezaei et al., 2015). The increase in T_g of the membranes indicates that the polymer chains variation of segmental mobility due to the incorporation of pillared nanoclays (Martin- Luengo et al., 1989). The fabricated PSf MMMs were glassy polymer in nature. T_g indicates the temperature at which the polymer changes into a rubbery nature by altering its properties. The matrix expands on transition, resulting in increased permeation rate of gasses through the membranes, and a resultant loss in the membrane selectivity, especially for CO_2 gas pairs (Yang et al., 2010). The P–C15A was observed to improve the thermal stability of the membranes slightly. The increase in T_g defines a structurally enhanced polymer region, occurring due to the stresses applied at membrane formation in the filler polymer interface (Valverde et al., 2005).

3.5. Gas permeability studies

3.5.1. Effect of P–C15A on gas transport properties

Gas permeation of neat and PSf/P–C15A MMMs were assessed in terms of gas permeability and selectivity for gas pairs (O_2/N_2 and CO_2/N_2). The permeance and the selectivity data were depicted in Fig. 10 and Fig. 11, respectively. The permeation of CO_2, N_2, and O_2 gases was increased with the increase in the loading percentage of PSf/P–C15A. Besides, the selectivity of O_2/N_2 and CO_2/N_2 gas pairs were decreased with an increase in P–C15A loading percentage. The relative increase in permeance for CO_2 from neat PSf to PSf/P–C15A (1 wt%) MMM, was about 232% from 21.68 to 72.04 GPU, while the CO_2/N_2 selectivity was decreased by 18.77% from 22.58 to 18.34. The corresponding increase in permeance for O_2 was 274% from 5.20 to 19.47 GPU with a drop of 9% in O_2/N_2 selectivity from 5.41 to 4.96. The complete data of permeance and selectivity for neat and MMMs is also presented as Table S1 in supplementary material.

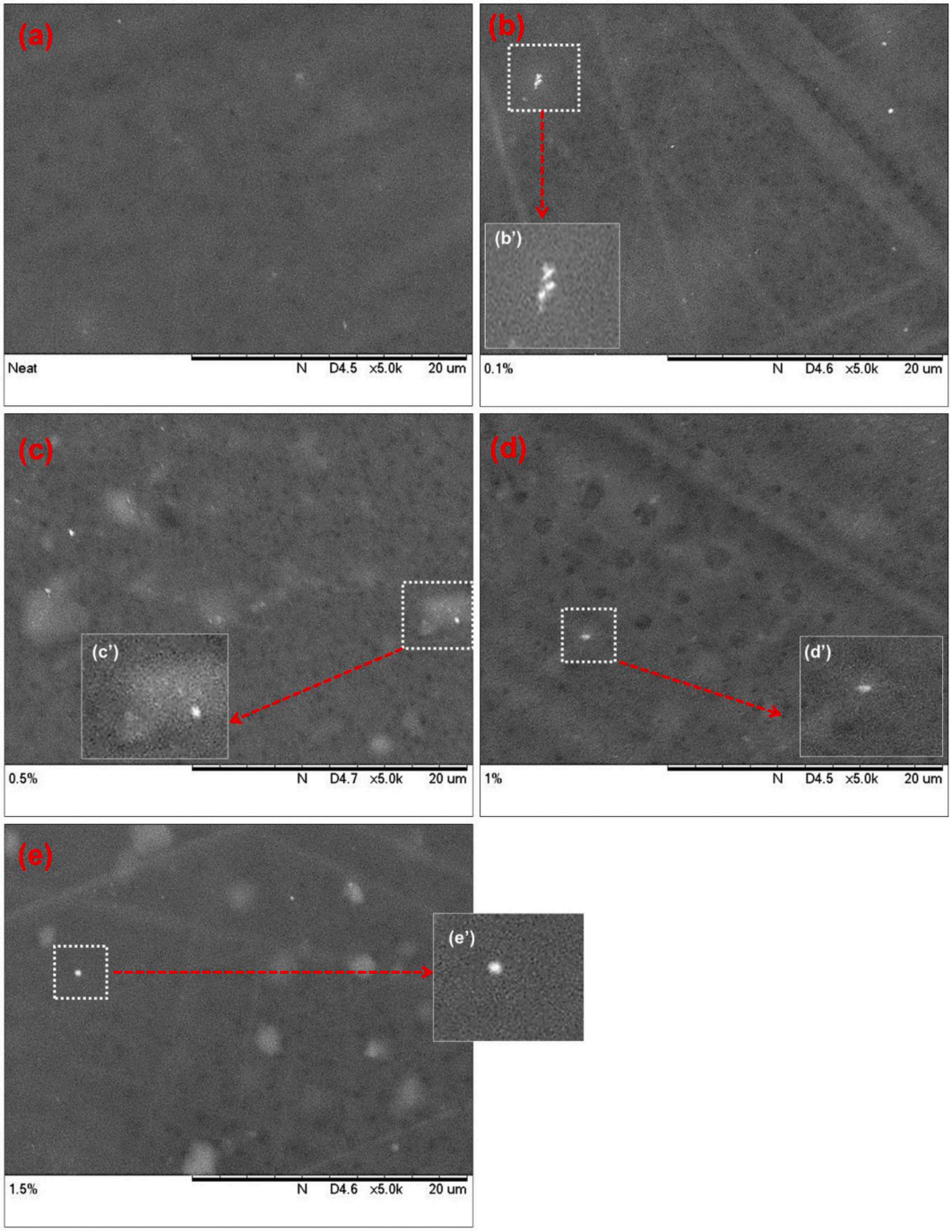

Fig. 6. Top surface morphology of membranes (a) Neat PSf (b) PSf/P–C15A (0.1 wt%) (c) PSf/P–C15A (0.5 wt%) (d) PSf/P–C15A (1 wt%) and (e) PSf/P–C15A (1.5 wt%).

In both neat PSf and PSf/P–C15A MMMs, the order of gas permeability was as follows: P (CO_2) > P (O_2) > P (N_2), was in consistent with most polymeric gas separation membranes (Ahn et al., 2008) (Jomekian et al., 2011a) (Matteucci et al., 2006). Gas permeability was decreased with the kinetic diameter and increased with condensability of the penetrant gas was reliable with glassy polymers (Matteucci et al., 2006) (Freeman et al., 2006). Kinetic diameter and gas condensability data were presented in Table 3 explains the gas permeability order (Sadeghi et al., 2010). The increase in gas permeation rate is attributed to the higher permeability via the pillared clay (P–C15A) present within PSf/P–C15A MMMs. P–C15A contributes increased in gas permeability due to the rise in micropore and total pore volume reported by Timofeeva et al. (2009). As depicted in Fig. 10, the permeation rate improvement for gases was similar up to P–C15A of 1 wt% loading, whereas the permeation increased significantly for PSf/P–C15A (1.5 wt %) MMMs, especially for slow permeable N_2 gas. This can be ascribed with the development of unselective voids at the PSf and P–C15A interface when the P–C15A loading increased to 1.5 wt% (Zulhairun et al., 2014). It was confirmed by the cross–sectional morphology of the PSf/P–C15A MMMs. The CO_2/N_2 and O_2/N_2 gas pair selectivities for PSf/P–C15A (0.1 wt %), PSf/P–C15A (0.5 wt %) and PSf/P–C15A (1 wt %) MMMs were similar to the neat membrane. (Fig. 11). Besides, the selectivity of O_2/N_2 and CO_2/N_2 gas pairs were decreased with an increase in P–C15A loading percentage to 1.5 wt% owing to better

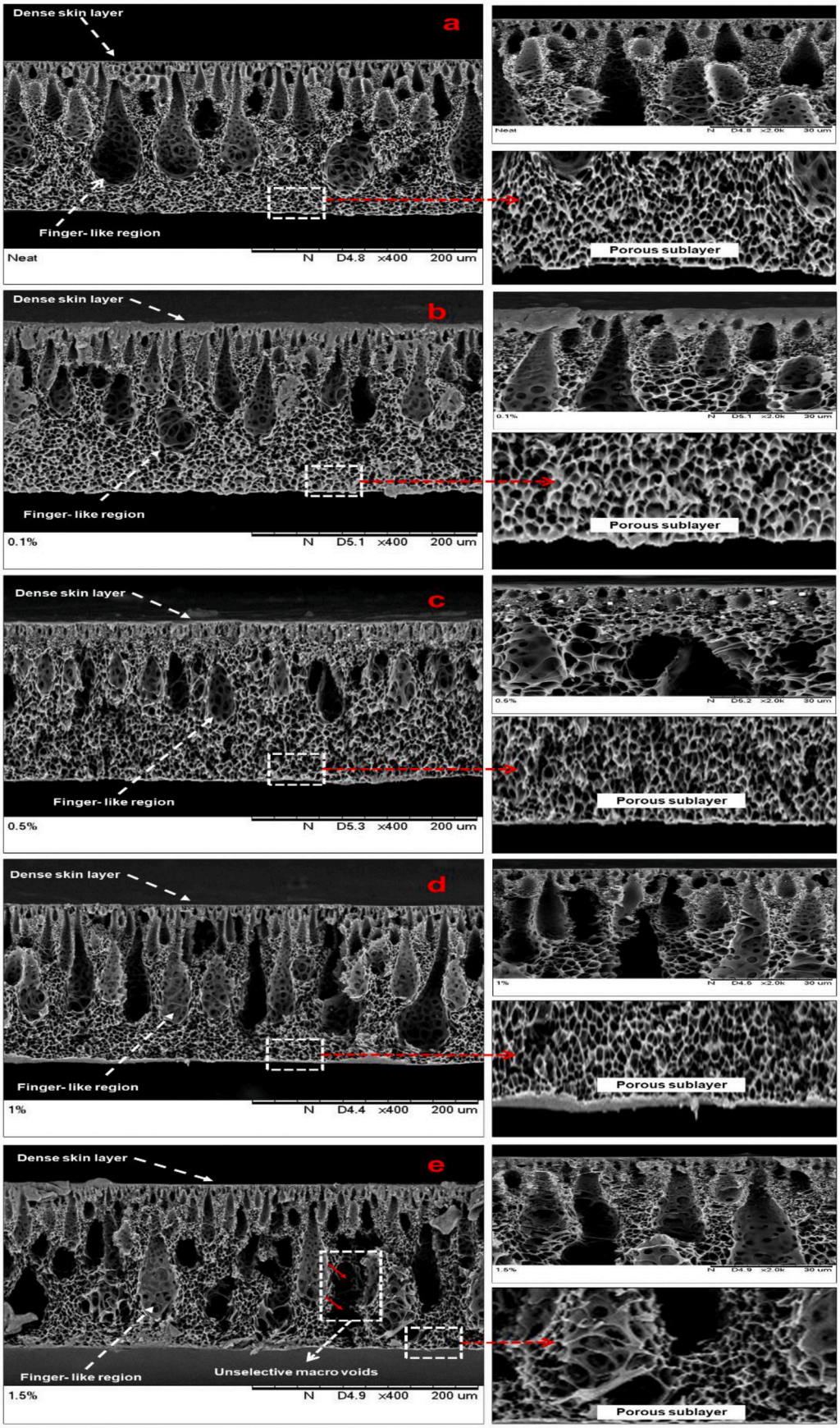

Fig. 7. Cross section morphology of membranes (a) Neat PSf (b) PSf/P–C15A (0.1 wt%) (c) PSf/P–C15A (0.5 wt%) (d) PSf/P–C15A (1 wt%) and (e) PSf/P–C15A (1.5 wt%).

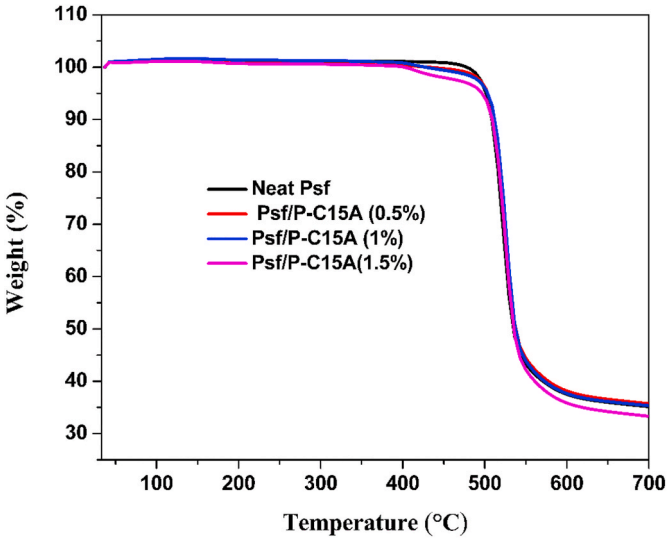

Fig. 8. TGA analysis of neat and PSf/P–C15A MMMs.

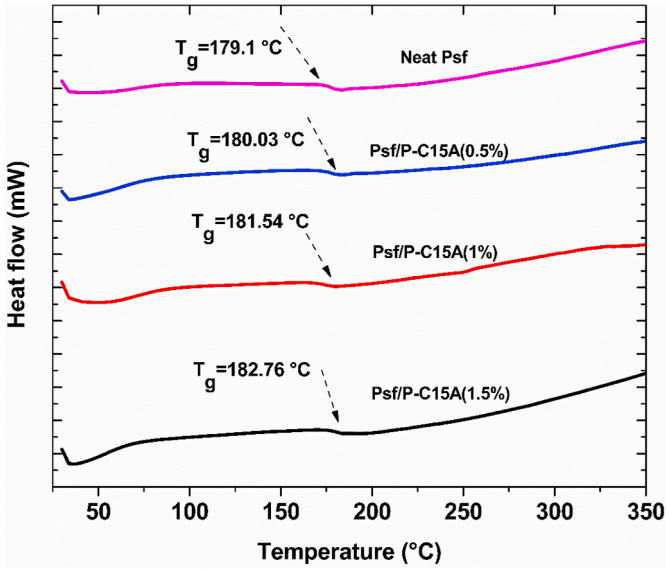

Fig. 9. DSC thermographs of neat and PSf/P–C15A MMMs.

enhancement in permeance of slow (N_2) gas than fast (O_2) gas permeation rate.

The PSf/P–C15A (1.5 wt%) MMM shown higher permeability with the lower selectivities for CO_2/N_2 and O_2/N_2 gas pairs compare to other fabricated membranes. The ability of PSf/P–C15A (1.5 wt%) MMM for discerning the permeance gas based on the kinematic diameter of gas molecule was diminished as the P–C15A loading increased within the membrane matrix. Thus, the PSf/P–C15A (1.5 wt%) MMM might permit the slow permeable (N_2) gas despite of gas kinematic diameter. This leads to higher permeance of N_2 gas via the PSf/P–C15A (1.5 wt%) MMM which results in decreased selectivites for CO_2/N_2 and O_2/N_2 gas pair. PSf/P–C15A (1 wt%) MMM exhibit better selectivity for gas pairs with reasonable permeability. Thus, the optimal loading of P–C15A within the fabricated PSf/P–C15A MMMs was found to be at 1 wt% loading. PSf/P–C15A (1 wt%) MMMs exhibit a significant increase in permeability, fractional decrease in selectivity, and driving the performance nearer to the Robeson upper bound. From the literature, it was understood that to show a similar improvement in permeability, inorganic fillers such as silica and MCM silicates need to be loaded at a high percentage (Jomekian et al., 2011b) (Jomekian et al., 2011a). At same conditions, 20 vol % silica added PSf membranes exhibit O_2/N_2 selectivity of 4.5 and O_2 permeability of 5, which was highly related to this study (Ahn et al., 2008). High filler loading leads to compromise of the structural integrity and possible filler agglomerations in the membrane microporous region (Moore and Koros, 2005). Hence P–C15A competes against other fillers even at a lower loading percentage and exhibits comparable results to the other fillers. Furthermore, to ensure reproducibility of fabrication method, the neat and PSf/P–C15A (1 wt%) MMMs were prepared again and their corresponding gas permeance and selectivity dataset were presented in Table S2 and S3, respectively.

3.5.2. *Comparison of fabricated MMMs with literature*

The fabricated MMMs were compared with literature to ascertain credibility and conformity. The properties of the fabricated MMMs are in concordance with published pre–existing data denoted in Table 4. The permeability of the asymmetric membranes was estimated by assuming an active skin layer thickness of 250 nm as commonly reported active layer thickness for asymmetric membranes (Zulhairun et al., 2014). The permeance and selectivity were compared with MCM–41/PSf membranes studied by Jomekian et al. (2011b), and Cloisite 15 A/PSf membranes investigated by Zulhairun et al. (2014) in Table 4. PSf/P–C15A MMMs were compared with other PSf membranes incorporated with other filler particles such as silica, and carbon nano–fibers reported by Ahn et al. (2008), and Jomekian et al. (2011a) in Table 5. The fabricated MMMs tend to show improved selectivity and permeability. The beneficial aspect was the enhanced properties exhibited with a mere 1% loading of P–C15A as compared to 20% silica loading. The requirement of low loading P–C15A can be attributed to the excellent compatibility between the pillared clay and PSf when compared to the higher loading fractions of inorganic silica (Ahn et al., 2008), and MCM fillers (Jomekian et al., 2011a) (Jomekian et al., 2011b).

3.6. *Robeson upper limit*

Polymeric membranes possessing maximum permeability and selectivity are more efficient and preferred for gas separations. However, experimentally membranes possessing higher permeability often show diminished selectivity, and the inverse also significant as mentioned by Robeson upper bound. The aforementioned upper bounds regarding the size–based segregation of gas molecules of various gas pairs have been found through experimental and further rationalized theoretically by utilizing pure gas data (Dehghani Kiadehi et al., 2015). The performance of neat and MMMs have been evaluated by plotting the permeability and selectivity of CO_2/N_2 and O_2/N_2 gas pairs against the Robeson upper bound (Rafizah and Ismail, 2008). This upper bound defines a trade–off between gas permeability and selectivity for various gas pairs. Since the establishment of the upper bound concept, numerous studies have aimed at solely achieving and exceeding the theoretical upper bound for various gases. The permeability of O_2 was plotted against O_2/N_2 selectivity with respect to Robeson upper bound is presented in Fig. 12(a), and similarly for CO_2/N_2 gas pairs in Fig. 12(b). In both cases, it was observed that with the addition of P–C15A filler, the MMMs advanced closer towards the Robeson upper bound and there was minimal loss of selectivity, while permeability increases significantly. From Fig. 12 (a) and 12 (b), it was found that the PSf/P–C15A (1 wt%) MMM performance with respect to Robeson upper bound was nearer to the PSf/P–C15A (0.5 wt%) MMM. Compared to 0.5 wt% P–C15A loaded PSf membrane, PSf/P–C15A (1 wt%) MMM exhibit reasonable selectivity with significant improvement in permeability for all gases. PSf/P–C15A (1 wt %) MMMs exhibit the greatest gas separation qualities, approaching closest to the Robeson upper bound for CO_2/N_2 and O_2/N_2 gas pairs. Hence, PSf/P–C15A (1 wt%) MMM was considered as efficient membrane for gas separation. Although the upper bound was not crossed in this experiment, significant information has been gained

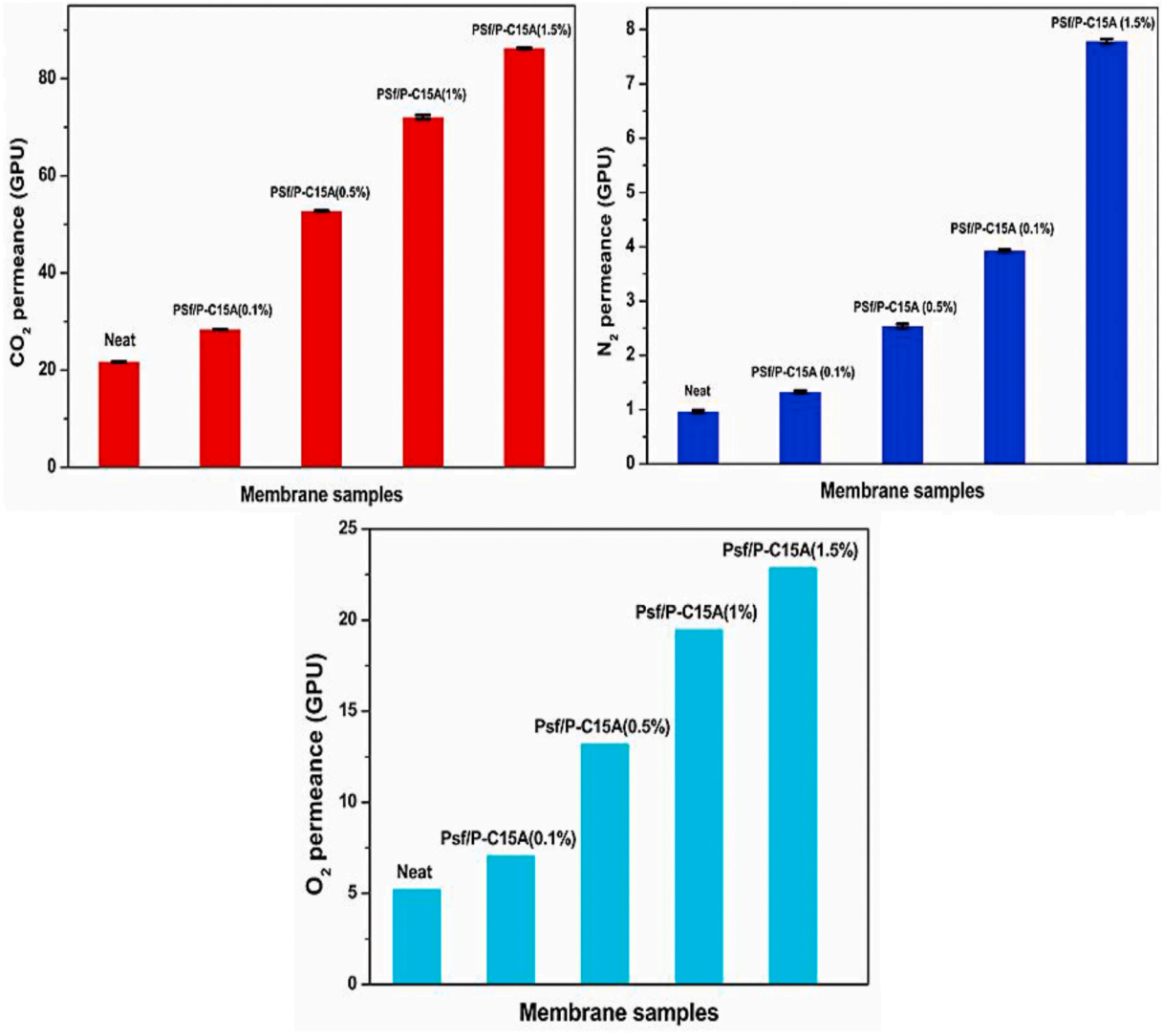

Fig. 10. Permeance of neat and PSf/P–C15A MMMs.

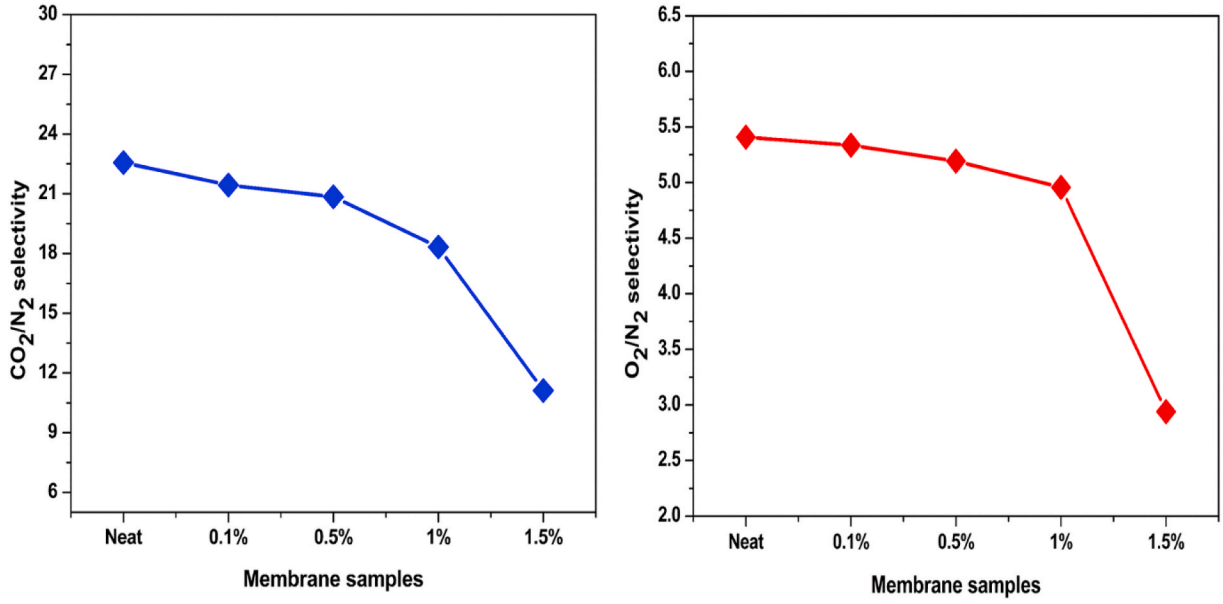

Fig. 11. Selectivity of neat and PSf/P–C15A MMMs for CO_2/N_2, and O_2/N_2 gas separation.

Table 3
Kinetic diameter and gas condensability of studied gases from literature (Sadeghi et al., 2010).

Gas	Kinetic Diameter (Å)	Condensability (K)
CO_2	3.30	195
O_2	3.46	107
N_2	3.64	71

Table 4
Comparison of O_2 and N_2 permeability and O_2/N_2 selectivity of fabricated MMMs with the reported values in literature with the reported values in literature.

Membrane	P_{O2} (GPU)	P_{N2} (GPU)	$\alpha_{O2/N2}$ (GPU)	Pressure (bar)	Reference
U MCM–41 (40 wt %)/PSF	10.46	2.6	4.02	4	Jomekian et al. (2011b)
U MCM–41 (20 wt %)/PSF	5.35	1.0	5.35	4	Jomekian et al. (2011b)
PSF –C15A (1.0 wt %)	16.37 ± 0.54	3.19 ± 0.21	5.13 ± 0.23	5	Zulhairun et al. (2014)
PSf/P–C15A (1.0 wt %)	19.47 ± 0.16	3.92 ± 0.08	4.96	4	This Study

on the applications of pillared Cloisite 15A (P–C15A) for membrane gas separation.

4. Conclusion

Inspired by the organic nature of C–15A, and the desired modifications offered by pillaring of clay filler, asymmetric P–C15A incorporated MMMs have been fabricated. The SEM images are in concordance with the findings and displayed an increase in fractional free volume with P–C15A. The experimental observations indicate a significant increase in membrane permeability at a low loading of P–C15A with an insignificant drop in permselectivity. The most efficient membrane was found to be at 1 wt % loading of P–C15A. A 274% increase was observed in the permeance of O_2 through the PSf/P–C15A (1 wt%) MMMs, with a decrease in O_2/N_2 selectivity of 9%. Also, a 240% increase in CO_2 permeability was found with a reduction in CO_2/N_2 selectivity of 18.5%. Hence, the overall efficiency of the membrane was found to be significantly increased. Further, the performance of neat and P–C15A incorporated MMMs were compared with the Robeson upper bound in terms of permeability and selectivity. The CO_2 permeability and the CO_2/N_2 and O_2/N_2 gas pairs selectivities of PSf/P–C15A (1 wt%) MMMs found to be approaching closer towards the Robeson upper bound. The increased permeability of the membranes with the P–C15A loading percentage could be attributed to the phase–separated dispersion state of the filler. Pillared clays are a relatively novel filler medium to be used in MMMs, and exhibit favorable compatible properties for gas separation. The study shows that there is a scope and potential application for the implementation of montmorillonite silicates with pillaring modification in gas separation.

Table 5
Comparison of CO_2 and N_2 permeability and CO_2/N_2 selectivity of fabricated MMMs with the reported values in literature.

Membrane samples	P_{O2} (Barrers)	P_{N2} (Barrers)	P_{CO2} (Barrers)	$\alpha_{O2/N2}$	$\alpha_{CO2/N2}$	Pressure (bar)	References
PSf/Silica (30.6 wt %)	5.0	1.12	19.7	4.46[a]	17.59[a]	4.45	Ahn et al. (2008)
CNF/PSF(1)	2.24	0.58	4.87	3.86	8.39	4	Dehghani Kiadehi et al. (2015)
PSF–CMS30 (30 wt %)	6.77 ± 0.01	1.82 ± 0.06	–	3.69	–	1.5	Rafizah and Ismail (2008)
MCM48/PSF (20 wt %)	1.90	0.38	–	5	–	4	Jomekian et al. (2011a)
PSf/P–C15A (1 wt %)	4.86 ± 0.04	0.98 ± 0.02	18.01 ± 0.10	4.96	18.34	4	This Study

[a] Calculated from permeability values of CO_2, O_2 and N_2.

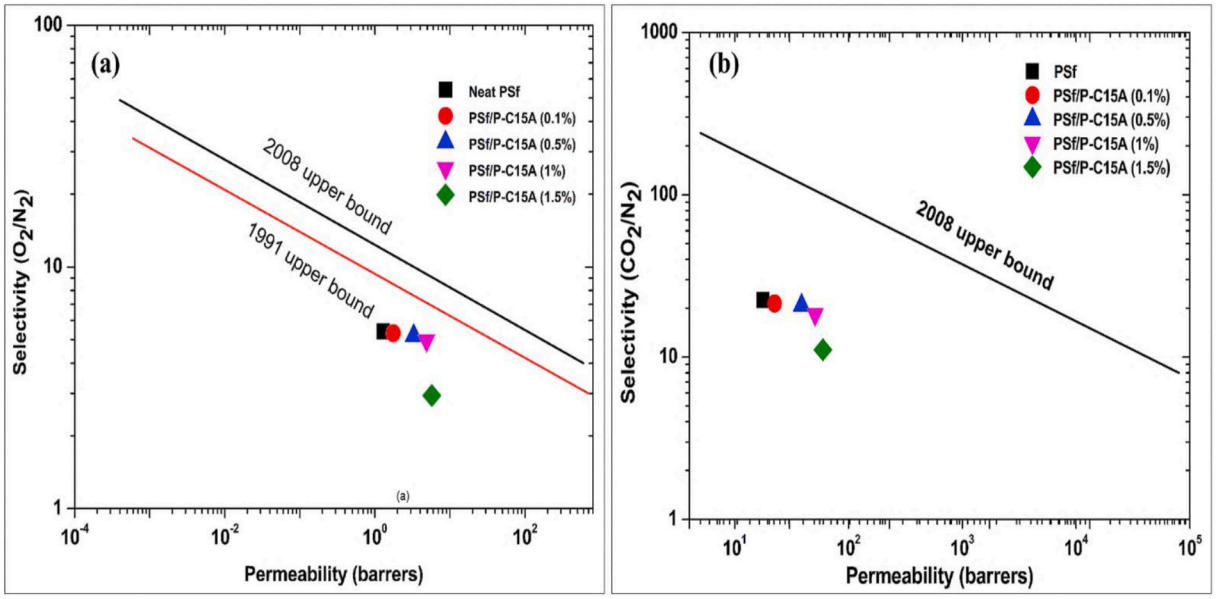

Fig. 12. Selectivity vs permeability graph plotted in comparison to the Robeson upper bound for (a) O_2/N_2 separation and (b) CO_2/N_2 separation.

Declaration of competing interest

The authors declare that they have no known competing financial interests or personal relationships that could have appeared to influence the work reported in this paper.

Acknowledgements

Authors G. Arthanareeswaran, S. Elakkiya, A. F. Ismail, Wirote Youravong and Erna Yuliwati acknowledge Science and Engineering Research Board (SERB) and ASEAN–India Science, Technology & Innovation Cooperation (AISTDF) for possible support under ASEAN and India research collaborative research project (IMRC/AISTDF/R&D/P–11/2018).

Nomenclature

C-15A	Cloisite 15A
Fe	Iron
P–C15A	Pillared Cloisite 15 A
CNTs	Carbon nanotubes
CMS	Carbon molecular sieves
MMT	Montmorillonite
PILCs	Pillared clays
PSf	Polysulfone
MMMs	Mixed matrix membranes
NaOH	Sodium hydroxide
$FeCl_3$	Ferric chloride
CO_2	Carbon dioxide
O_2	Oxygen
N_2	Nitrogen
THF	Tetrahydrafuran
NMP	N-methyl-2-pyrrolidone
PDMS	Polydimethylsiloxane
SEM	Scanning Electron Microscope
EDAX	Energy Dispersive X-ray Spectroscopy
TGA	Thermogravimetric Analysis
DSC	Differential Scanning Calorimeter
T_g	Glass transition temperature (°C)
ΔP	Pressure (cmHg)
ΔT	Temperature (°C)
P_i	Permeability of gas through cross section of membrane (Barrer)
l	Skin thickness of the membrane (cm)
$Pi/1$	Permeance of gas through unit length of membrane cross section (GPU)
Q	Flow rate of gas entering (cm^3,STP/s)
A	Surface area of the membrane (cm^2)
$\alpha_{a/b}$	Selectivity of gas pairs
Pa/l	Permeance of the first gas through the membrane
Pb/l	Permeance of the second gas through the membrane

Appendix A. .Supplementary data

Supplementary data to this article can be found online at https://doi.org/10.1016/j.jngse.2020.103720.

References

Ahn, J., Chung, W.J., Pinnau, I., Guiver, M.D., 2008. Polysulfone/silica nanoparticle mixed-matrix membranes for gas separation. J. Membr. Sci. 314, 123–133. https://doi.org/10.1016/j.memsci.2008.01.031.

Aroon, M.A., Ismail, A.F., Montazer-Rahmati, M.M., Matsuura, T., 2010. Morphology and permeation properties of polysulfone membranes for gas separation: effects of non-solvent additives and co-solvent. Separ. Purif. Technol. 72, 194–202. https://doi.org/10.1016/j.seppur.2010.02.009.

Dai, Z., Noble, R.D., Gin, D.L., Zhang, X., Deng, L., 2016. Combination of ionic liquids with membrane technology: a new approach for CO2 separation. J. Membr. Sci. 497, 1–20. https://doi.org/10.1016/j.memsci.2015.08.060.

Dehghani Kiadehi, A., Rahimpour, A., Jahanshahi, M., Ghoreyshi, A.A., 2015. Novel carbon nano-fibers (CNF)/polysulfone (PSf) mixed matrix membranes for gas separation. J. Ind. Eng. Chem. 22, 199–207. https://doi.org/10.1016/j.jiec.2014.07.011.

Fattahi, M., Kazemeini, M., Khorasheh, F., Rashidi, A.M., 2015. Morphological investigations of nanostructured V_2O_5 over graphene used for the ODHP reaction: from synthesis to physiochemical evaluations. Catal. Sci. Technol. 5, 910–924. https://doi.org/10.1039/C4CY01108B.

Freeman, B., Yampolskii, Y., Pinnau, I. (Eds.), 2006. Materials Science of Membranes for Gas and Vapor Separation. John Wiley & Sons.

Ghasemipour, P., Fattahi, M., Rasekh, B., Yazdian, F., 2020. Developing the ternary ZnO doped MoS 2 nanostructures grafted on CNT and reduced graphene oxide (RGO) for photocatalytic degradation of aniline. Sci. Rep. 1–16. https://doi.org/10.1038/s41598-020-61367-7.

Gil, A., Vicente, M.A., Korili, S.A., 2005. Effect of the Si/Al ratio on the structure and surface properties of silica-alumina-pillared clays. J. Catal. 229, 119–126. https://doi.org/10.1016/j.jcat.2004.10.013.

Guo, F., Aryana, S., Han, Y., Jiao, Y., 2018. A review of the synthesis and applications of polymer-nanoclay composites. Appl. Sci. 8, 1–29. https://doi.org/10.3390/app8091696.

Hashemifard, S.A., Ismail, A.F., Matsuura, T., 2011. Effects of montmorillonite nano-clay fillers on PEI mixed matrix membrane for CO2 removal. Chem. Eng. J. 170, 316–325. https://doi.org/10.1016/j.cej.2011.03.063.

Herrera-Alonso, J.M., Marand, E., Little, J.C., Cox, S.S., 2009. Transport properties in polyurethane/clay nanocomposites as barrier materials: effect of processing conditions. J. Membr. Sci. 337, 208–214. https://doi.org/10.1016/j.memsci.2009.03.045.

Hosseini, S.S., Li, Y., Chung, T.S., Liu, Y., 2007. Enhanced gas separation performance of nanocomposite membranes using MgO nanoparticles. J. Membr. Sci. 302, 207–217. https://doi.org/10.1016/j.memsci.2007.06.062.

Ismail, A.F., Lai, P.Y., 2003. Effects of phase inversion and rheological factors on formation of defect-free and ultrathin-skinned asymmetric polysulfone membranes for gas separation. Separ. Purif. Technol. 33, 127–143. https://doi.org/10.1016/S1383-5866(02)00201-0.

Ismail, A.F., Goh, P.S., Sanip, S.M., Aziz, M., 2009. Transport and separation properties of carbon nanotube-mixed matrix membrane. Separ. Purif. Technol. 70, 12–26. https://doi.org/10.1016/j.seppur.2009.09.002.

Johnson, J.W., Brody, J.F., Soled, S.L., Gates, W.E., Robbins, J.L., Marucchi-Soos, E., 1996. Controlling the chemistry of the micropore volume in pillared clays and micas. J. Mol. Catal. Chem. 107, 67–73. https://doi.org/10.1016/1381-1169(95)00228-6.

Jomekian, A., Mansoori, S.A.A., Monirimanesh, N., Shafiee, A., 2011a. Gas transport behavior of DMDCS modified MCM-48/polysulfone mixed matrix membrane coated by PDMS. Kor. J. Chem. Eng. 28, 2069–2075. https://doi.org/10.1007/s11814-011-0075-8.

Jomekian, A., Pakizeh, M., Shafiee, A.R., Mansoori, S.A.A., 2011b. Fabrication or preparation and characterization of new modified MCM-41/PSf nanocomposite membrane coated by PDMS. Separ. Purif. Technol. 80, 556–565. https://doi.org/10.1016/j.seppur.2011.06.011.

Kim, S., Chen, L., Johnson, J.K., Marand, E., 2007. Polysulfone and functionalized carbon nanotube mixed matrix membranes for gas separation: theory and experiment. J. Membr. Sci. 294, 147–158. https://doi.org/10.1016/j.memsci.2007.02.028.

Kurian, M., Babu, R., 2013. Iron aluminium mixed pillared montmorillonite and the rare earth exchanged analogues as efficient catalysts for phenol oxidation. J. Environ. Chem. Eng. 1, 86–91. https://doi.org/10.1016/j.jece.2013.04.005.

Li, J., Hu, M., Zuo, S., Wang, X., 2018. Catalytic combustion of volatile organic compounds on pillared interlayered clay (PILC)-based catalysts. Curr. Opin. Chem. Eng. 20, 93–98. https://doi.org/10.1016/j.coche.2018.02.001.

Mandalia, T., Crespin, M., Messad, D., Bergaya, F., 1998. Large interlayer repeat distances observed for montmorillonites treated by mixed Al-Fe and Fe pillaring solutions. Chem. Commun. 2, 2111–2112. https://doi.org/10.1039/a803746i.

Martin- Luengo, M.A., Martins-Carvalho, H., Ladriere, Jean, Grange, Paul, 1989. Fe (III)-pillared montmorillonites: preparation and characterization. Clay Miner. 24 (3), 495–504. https://doi.org/10.1180/claymin.1989.024.3.03.

Matteucci, S., Yampolskii, Y., Freeman, B.D., Pinnau, I., 2006. Transport of gases and vapors in glassy and rubbery polymers. Materials science of membranes for gas and vapor separation 1, 1–2. https://doi.org/10.1002/047002903X.ch1.

Mnasri-Ghnimi, S., Frini-Srasra, N., 2014. Promoting effect of cerium on the characteristic and catalytic activity of Al, Zr, and Al-Zr pillared clay. Appl. Clay Sci. 88–89, 214–220. https://doi.org/10.1016/j.clay.2013.10.030.

Moaddeb, M., Koros, W.J., 1997. Gas transport properties of thin polymeric membranes in the presence of silicon dioxide particles. J. Membr. Sci. 125, 143–163. https://doi.org/10.1016/S0376-7388(96)00251-7.

Moore, T.T., Koros, W.J., 2005. Non-ideal effects in organic-inorganic materials for gas separation membranes. J. Mol. Struct. 739, 87–98. https://doi.org/10.1016/j.molstruc.2004.05.043.

Pandey, P., Chauhan, R.S., 2001. Membranes for gas separation. Prog. Polym. Sci. 26, 853–893. https://doi.org/10.1016/S0079-6700(01)00009-0.

Park, J.Y., Paul, D.R., 1997. Correlation and prediction of gas permeability in glassy polymer membrane materials via a modified free volume based group contribution method. J. Membr. Sci. 125, 23–39. https://doi.org/10.1016/S0376-7388(96)00061-0.

Pechar, T.W., Kim, S., Vaughan, B., Marand, E., Tsapatsis, M., Jeong, H.K., Cornelius, C. J., 2006. Fabrication and characterization of polyimide-zeolite L mixed matrix membranes for gas separations. J. Membr. Sci. 277, 195–202. https://doi.org/10.1016/j.memsci.2005.10.029.

Rafizah, W.A.W., Ismail, A.F., 2008. Effect of carbon molecular sieve sizing with poly (vinyl pyrrolidone) K-15 on carbon molecular sieve-polysulfone mixed matrix membrane. J. Membr. Sci. 307, 53–61. https://doi.org/10.1016/j.memsci.2007.09.007.

Rezaee, M., Kazemeini, M., Fattahi, M., Rashidi, A.M., Vafajoo, L., 2016. Oxidation of H2S to elemental sulfur over alumina-based nanocatalysts: synthesis and physiochemical evaluations. Sci. Iran. 23, 1160–1174.

Rezaei, M., Ismail, A.F., Bakeri, G., Hashemifard, S.A., Matsuura, T., 2015. Effect of general montmorillonite and Cloisite 15A on structural parameters and performance of mixed matrix membranes contactor for CO2 absorption. Chem. Eng. J. 260, 875–885. https://doi.org/10.1016/j.cej.2014.09.027.

Robeson, L.M., 2008. The upper bound revisited. J. Membr. Sci. 320, 390–400. https://doi.org/10.1016/j.memsci.2008.04.030.

Sadeghi, M., Ali, M., Barikani, M., Ghalei, B., 2010. The effect of urethane and urea content on the gas permeation properties of poly (urethane-urea) membranes. J. Membr. Sci. 354, 40–47. https://doi.org/10.1016/j.memsci.2010.02.070.

Sasikumar, B., Arthanareeswaran, G., Ismail, A.F., 2018. Recent progress in ionic liquid membranes for gas separation. J. Mol. Liq. 266, 330–341. https://doi.org/10.1016/j.molliq.2018.06.081.

Sasikumar, B., Arthanareeswaran, G., Sankaranarayanan, K., Jeyadheepan, K., 2019. Synthesis and formation of phase-tuned TiO2-/ionic liquid-incorporated polymeric membranes for ammonia sensing at room temperature. ACS Sustain. Chem. Eng. https://doi.org/10.1021/acssuschemeng.9b01850.

Tantekin-Ersolmaz, Ş.B., Atalay-Oral, Ç., Tatlıer, M., Erdem-Şenatalar, A., Schoeman, B., Sterte, J., 2000. Effect of zeolite particle size on the performance of polymer–zeolite mixed matrix membranes. J. Membr. Sci. 175 (2), 285–288.

Timofeeva, M.N., Khankhasaeva, S.T., V Badmaeva, S., Chuvilin, A.L., 2005. Synthesis , characterization and catalytic application for wet oxidation of phenol of iron-containing clays, 59, 243–248. https://doi.org/10.1016/j.apcatb.2005.01.013.

Timofeeva, M.N., Khankhasaeva, S.T., Chesalov, Y.A., V Tsybulya, S., 2009. Applied catalysis B : environmental synthesis of Fe , Al-pillared clays starting from the Al , Fe-polymeric precursor. Effect of synthesis parameters on textural and catalytic properties 88, 127–134. https://doi.org/10.1016/j.apcatb.2008.09.013.

Unnikrishnan, L., Mohanty, S., Nayak, S.K., Singh, N., 2012. Synthesis and characterization of polysulfone/clay nanocomposite membranes for fuel cell application. J. Appl. Polym. Sci. https://doi.org/10.1002/app.34355, 2012.

Usman, M., Ahmed, A., Yu, B., Peng, Q., Shen, Y., 2019. A review of different synthetic approaches of amorphous intrinsic microporous polymers and their potential applications in membrane-based gases separation. Eur. Polym. J. 120, 109262. https://doi.org/10.1016/j.eurpolymj.2019.109262.

Valverde, J.L., Romero, A., Romero, R., García, P.B., Sánchez, M.L., Asencio, I., 2005. Preparation and characterization of Fe-PILCs. Influence of the synthesis parameters. Clay Clay Miner. 53, 613–621. https://doi.org/10.1346/CCMN.2005.0530607.

Vercauteren, S., Luyten, J., Leysen, R., Vansant, E.F., 1996. Synthesis and characterization of a pillared clay membrane. J. Membr. Sci. 119, 161–168.

Vercauteren, S., Vayer, M., Van Damme, H., Luyten, J., Leysen, R., Vansant, E.F., 1998. The preparation and characterization of ceramic membranes with a pillared clay top layer. Colloid. Surface. Physicochem. Eng. Aspect. 138, 367–376. https://doi.org/10.1016/S0927-7757(97)00143-X.

Vu, D.Q., Koros, W.J., Miller, S.J., 2002. High pressure CO_2/CH_4 separation using carbon molecular sieve hollow fiber membranes. Ind. Eng. Chem. Res. 41, 367–380. https://doi.org/10.1021/ie010119w.

Yang, Z., Peng, H., Wang, W., Liu, T., 2010. Effect of fractional free volume and Tg on gas separation through membranes made with different glassy polymers. J. Appl. Polym. Sci. 116, 2658–2667. https://doi.org/10.1002/app.

Zulhairun, A.K., Ismail, A.F., 2014. The role of layered silicate loadings and their dispersion states on the gas separation performance of mixed matrix membrane. J. Membr. Sci. 468, 20–30. https://doi.org/10.1016/j.memsci.2014.05.038.

Zulhairun, A.K., Ismail, A.F., Matsuura, T., Abdullah, M.S., Mustafa, A., 2014. Asymmetric mixed matrix membrane incorporating organically modified clay particle for gas separation. Chem. Eng. J. 241, 495–503. https://doi.org/10.1016/j.cej.2013.10.042.